Journal of Applied Physics

Metallization of ZnSb and contact resistance

Cite as: J. Appl. Phys. **130**, 025107 (2021); https://doi.org/10.1063/5.0043958
Submitted: 12 January 2021 . Accepted: 20 June 2021 . Published Online: 12 July 2021

X. Song, H. Riis, Ø. Prytz, and T. G. Finstad

Journal of Applied Physics ARTICLE scitation.org/journal/jap

Metallization of ZnSb and contact resistance

Cite as: J. Appl. Phys. **130**, 025107 (2021); doi: 10.1063/5.0043958
Submitted: 12 January 2021 · Accepted: 20 June 2021 ·
Published Online: 12 July 2021

View Online Export Citation CrossMark

X. Song, H. Riis, Ø. Prytz, and T. G. Finstad[a)]

AFFILIATIONS

Center of Material Science and Nanotechnology and Department of Physics, University of Oslo, Oslo, Norway

[a)]**Author to whom correspondence should be addressed:** terje.finstad@fys.uio.no

ABSTRACT

We present results on electrical resistance of metal contacts to ZnSb. We synthesized the thermoelectric semiconductor ZnSb with specific doping concentrations by adding Cu as an acceptor to the melt, followed by solidification, crushing, ball-milling, hot-pressing, sawing, and polishing yielding wafers suitable for substrates for further processing. Many batches were made yielding different doping concentrations. We defined transmission line geometries in deposited metal films for specific contact resistance measurements. We prepared sets of Cu, Ti, and Ni films, respectively. We measured the contact resistance vs annealing temperatures. For Cu/ZnSb samples, we observed a specific contact resistance from 5×10^{-7} to $4 \times 10^{-5}\ \Omega\,\mathrm{cm}^2$. We also measured the carrier concentration of ZnSb. The measurement data of the specific contact resistance had systematic dependence on doping concentration and annealing temperature and were analyzed by a model incorporating different transport mechanisms across the energy barrier at the metal–semiconductor interface. The data were discussed in terms of systematic variation in barrier height and density of states effective mass. We proposed these arising as a consequence of interactions at the interface and a nonparabolic valence band. We have also monitored the interface of the ZnSb substrate and metal films with transmission electron microscopy.

I. INTRODUCTION

Thermoelectric modules made by the semiconductor material ZnSb were used a long time ago,[1] and a patent for improving them dates back to 1870.[2] In recent decades, both the electrical properties and thermal properties of the material have been improved, which can be attributed to the introduction of proper doping and nanostructuring.[3] Thermoelectrical materials are commonly rated by their standard figure of merit,[4] zT. ZnSb with zT around 1, and even above in a few studies, have been reported.[3,5–8] The underlying improvements have remade ZnSb a promising thermoelectric material for energy harvesting.[6,9] Yet, it is important to consider that the actual performance of a device depends on many other factors than the material parameter zT. For example, the contact metallization is essential and has several requirements for practical use. It has to be optimized with respect to factors such as thermal stress, heat distribution, long term durability, stability with respect to the environment, and, of course, the contact resistance. Metal contacts on thermoelectrics are closely related to the material science going into the thermoelectric material itself; yet, the topic has been paid surprisingly little attention in the literature on thermoelectric materials and devices. Different metallization techniques have been investigated for other thermoelectric materials. For instance, electroplating followed by thermo-compression bonding has been reported for indium contacts with nickel diffusion barriers on Bi_2Te_3,[10] while Shtern *et al.*[11] reported on the optimization of evaporated Ni films for contacts to $Bi_{0.5}Sb_{1.5}Te_3$ and $Bi_2Te_{2.8}Se_{0.2}$, and Jung *et al.*[12] presented a review on the lead free transient liquid phase soldering addressing thermoelectrics. Yet, there are only a few reports on the metallization of ZnSb.[13,14]

In this work, we report on metal films to ZnSb and verify a methodology for measuring contact resistance. In Sec. II A, we analyze how small the specific contact resistance needs to be for a practical thermoelectrical module. Then, in Sec. II B, we present the theoretical background and model of a metal–semiconductor junction which we use to analyze the contact resistance measurements. The motivation for the choices is presented in Sec. II C, while details on the experiments and materials are presented in Sec. III. Results are presented and discussed in Sec. IV, mainly on Cu/ZnSb (Sec. IV A), but also Ti/ZnSb and Ni/ZnSb (Sec. IV B). The conclusion follows in Sec. V.

II. ANALYSIS AND THEORY

A. Power loss by contacts

The contact resistance strongly influences the performance of a thermoelectric module. To illustrate how much a given contact

resistance influence the efficiency, we here present calculations of the power loss at the contacts for a model thermoelectric device made from ZnSb. A simplified thermoelectric generator (TEG) with 200 pairs of legs and its equivalent electric circuit are sketched in Fig. 1(a). The legs are bar-shaped pieces of n- and p-type semiconductor with a conducting metal layer at both ends of the bar creating an electrical serial connection, while the legs are thermally in parallel. Each semiconductor–metal junction contributes a contact resistance equal to $\rho_c \times A$, where ρ_c is the specific contact resistivity and A is the area. The p- and n-type materials are assumed to have thermoelectric properties similar to ZnSb. Both electrical and thermal properties in these calculations are empirical

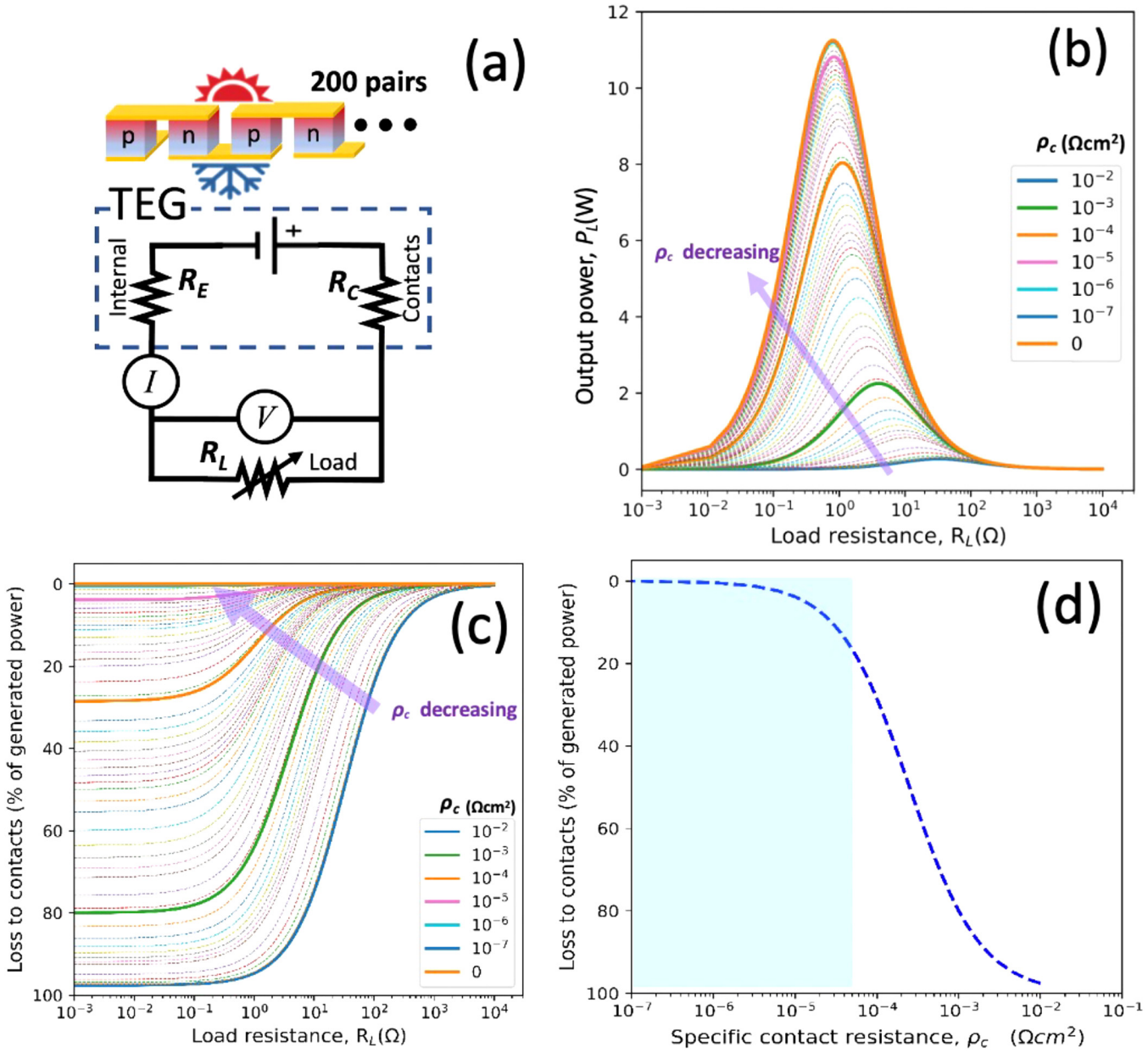

FIG. 1. Power estimate for a thermoelectric generator (TEG). (a) Equivalent electrical circuit of a TEG connected to a load resistor, R_L. Here, R_C represents the contact resistances and R_E represents the internal resistance of all elements not including contacts. (b) Power delivered to the load as a function of R_L with the specific contact resistivity, ρ_c, of each contact as a parameter. (c) Power loss to the contacts relative to the total power generated as a function of R_L with ρ_c as a parameter. (d) Power loss to the contacts in percent of the total loss in the TEG as a function of ρ_c.

data, which can be found in previous studies.[15] The dimension of each leg is $5 \times 5 \times 5\ \text{mm}^3$ and an environment temperature of 250 °C is used, which is within the temperature range where ZnSb has a decent performance. The electrical potential generated by a temperature difference of 50 K over the legs, V_T, is 6 V, and the internal resistance of all elements not including contacts, R_E, is 0.8 Ω. When the temperature gradient generates an electrical potential in the thermoelectric device, the power loss at the contacts will depend on the electric current through this circuit, and the current depends on the load resistance, R_L. Figure 1(b) shows how the output power of the TEG varies with R_L. Each curve is for a different total contact resistance, R_C corresponding to a different ρ_c ranging from 0 to $10^{-2}\ \Omega\,\text{cm}^2$. The maximum output power of the TEG is limited by R_E and R_C. Figure 1(c) shows how large percentage of the total generated power is lost in the contacts as a function of R_L with ρ_c as a parameter. Figure 1(d) shows the percentage of the total loss in the TEG that is lost by the contacts as a function of the contact resistivity. From this curve, we see that in order to keep the power loss at the contacts lower than 20%, the specific contact resistance should be in the range 10^{-7}–$10^{-5}\ \Omega\,\text{cm}^2$, given the thermoelectric properties of ZnSb.

B. Model for carrier transport across metal–semiconductor interface

Metal–semiconductor (MS) junctions have great importance in all electrical devices and have been under intense study for more than 70 years.[16] In general, a MS junction has a nonlinear current voltage characteristic due to an energy barrier for the carriers around the interface. It behaves as a Schottky barrier rectifier for low doping; for high doping, it has an insignificant voltage drop across the barrier (and then nonlinearity and rectification are insignificant). The energy bands of a metal–ZnSb interface are drawn schematically in Fig. 2 for three different doping concentrations.

Figure 2(a) shows the case for light doping. The dominating transport mechanism of charge carriers for the junction, made up of p-type ZnSb and the metal, is by thermionic emission, TE. That is thermal excitation of carriers over the barrier drawn by an arrow in Fig. 2(a) (considering that the kinetic energy of a hole is measured from the edge of the valence band and downwards). For the medium doping case shown in Fig. 2(b), the dominating transport between the materials is by thermal field emission, TFE. Here, the carriers are thermally excited and then pass through the energy barrier at a location where it is sufficiently thin that tunneling is more probable than excitation over the barrier. For heavy doping as shown in Fig. 2(c) one has field emission, FE, and then holes tunnel through the barrier at the Fermi level. These three transport mechanisms have been described by models. We will use the model as described by Yu.[17] The model considers the functional dependence of the current density, J, and the specific contact resistance, ρ_c (also called contact resistivity) by the common definition given by

$$\rho_c = \left.\frac{\partial V}{\partial J}\right|_{V\to 0} \propto \begin{cases} \exp\left(\dfrac{\phi_B}{kT}\right) & \text{thermionic emission (TE)}, \\ \exp\left(\dfrac{\phi_B}{(\sqrt{N_A})_{\coth}\left(\frac{E_{00}}{kT}\right)}\right) & \text{thermionic field emission (TFE)}, \\ \exp\left(\dfrac{\phi_B}{E_{00}}\right) & \text{field emission (FE)}. \end{cases} \tag{1}$$

Here, the main dependence is by the barrier height, Φ_B, and the acceptor doping concentration N_A. The variable E_{00} is defined by

$$E_{00} = \frac{q\hbar}{2}\sqrt{\frac{N_A}{m^*\epsilon}}, \tag{2}$$

where m^* is the density of state effective mass and the other symbols have their usual meaning. The barrier height Φ_B will, of course, be the barrier for holes Φ_{Bp}. Equation (1) shows how the contact resistance will vary with acceptor concentration, N_A, and barrier height Φ_{Bp} for the regimes dominated by TE, TFE, or FE. It should be intuitive that a low contact resistance requires a low barrier Φ_{Bp} and a narrow barrier and the latter can be achieved by a high doping concentration N_A. Usually, the doping concentration for optimized thermoelectric performance will be on the heavy doping side of the "doping-scale," which is fortunate for overall optimization purposes.

C. Motivation for selection of metal to thermoelectric ZnSb

There is no proven safe strategy to achieve a very low Φ_B. The barrier is dependent upon the interaction of atoms at the interface[16] which is complicated to model. There are trends, but these have exceptions on a case-by-case basis. Some of the empirical relationships rely on differences in work function between materials and electronegativity differences. For the case of ZnSb, the work function and the electron affinity have not been determined experimentally, and experimental data on the barrier height between ZnSb and metals are totally lacking.

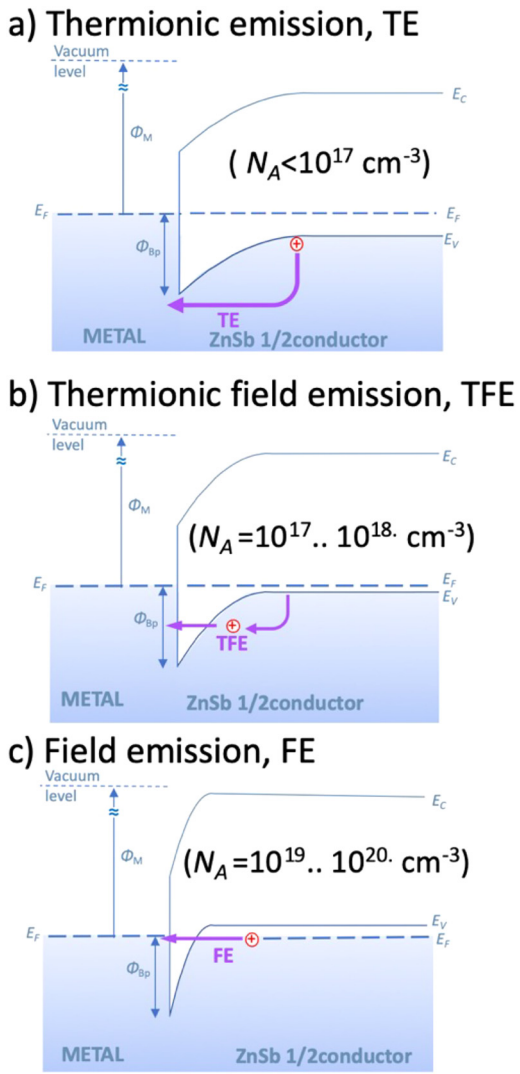

FIG. 2. Schematic figure of the energy band diagram of a metal–ZnSb interface. Here, Φ_{Bp} is the barrier height for holes, Φ_M is the metal work function, E_c and E_v are the edges of the conduction band and valence band, respectively. The figure shows the dominating transport of holes for three cases of acceptor doping concentration N_A: (a) Light doping. Thermionic emission dominates as in a Schottky barrier. (b) Medium doping. Thermionic-field emission dominates. The carriers are here thermally excited to an energy for which the tunnel barrier is thin enough that we get appreciable thermionic-field emission, TFE. (c) Heavy doping. We have tunneling at the Fermi level. This is field emission, FE.

The above arguments show that the investigation of the interface between any metal and ZnSb would be interesting from an academic point of view. Furthermore, it may be of particular technological significance to study the interface between Cu and ZnSb as Cu may be one of the main constituents in a metallization system for ZnSb. Cu has low cost, and the technology for bonding patterns to insulator substrates like alumina is well established. The thermal expansion of Cu matches that of ZnSb, and Cu is a p-type dopant in ZnSb.[3] Thus, Cu diffusion into ZnSb might be beneficial for both contact resistance and thermoelectric parameter optimization. Here, we aim for the best controlled experiments and models in order to understand the fundamental mechanisms. Thus, we study one metal at a time (no diffusion barriers, or wetting layers) and in a manner that should yield an intimate contact between metal and ZnSb. The latter would traditionally be by metal evaporation. Furthermore, although it is beyond the scope of this paper, the microstructure changes at the interface will also give some hint for the particulars of Cu in contact with ZnSb. For comparison, we also show results of ZnSb with Ti and Ni depositions that are also common contact materials for semiconductor applications.

III. EXPERIMENTAL DETAILS

Wafers of the semiconductor material ZnSb ware made from the elements by a procedure described earlier.[15] The Cu dopant concentrations were 0, 0.05, 0.075, and 0.1 at. %. The procedure ending with hot-pressing of ball-milled ZnSb powder was followed by cutting and polishing to make suitable substrates for metal film depositions. The contact patterns were created by using shadow masks during depositions. The shadow masks had been made by a laser cutter. Metal films of Cu, Ti, or Ni were deposited on different ZnSb substrates in the UiO MiNaLab clean room facility.[18] The Cu films were deposited by e-beam evaporation and sputter deposition, while Ti and Ni were deposited by e-beam evaporation only. The thickness of the films was between 30 and 900 nm for different depositions. After the deposition, the samples were annealed for 3 h at different temperatures under a controlled Ar flow to investigate the effect of the heat treatment.

Figure 3 shows the details of the samples and the measurements of the contact resistivity using the transmission line method (TLM).[19] Figure 3(a) shows the metal lines created by using the shadow mask. They have different separation. Measuring the resistance as a function distance yield a straight line with a slope giving the semiconductor resistance and an intercept with the abscissa giving the contact resistance. We also measured the carrier concentration of the sample by Hall effect measurements at room temperature.

IV. RESULTS AND DISCUSSION

A. Interface characterization by TEM

The interface between the metal and the ZnSb substrate was characterized by transmission electron microscopy (TEM). For some Cu films evaporated by e-beam, we observed gaps in the Cu/ZnSb interface, as shown in Fig. 4(a). This indicates poor adhesion between the ZnSb substrate and the Cu film, which then do not fulfill our requirement for the study of an intimate contact between the metal and ZnSb, and the TEM monitoring of the evaporations have a good quality assurance. For Cu, we in the remainder only include sputter deposited films which by TEM appears smooth without visible gaps as

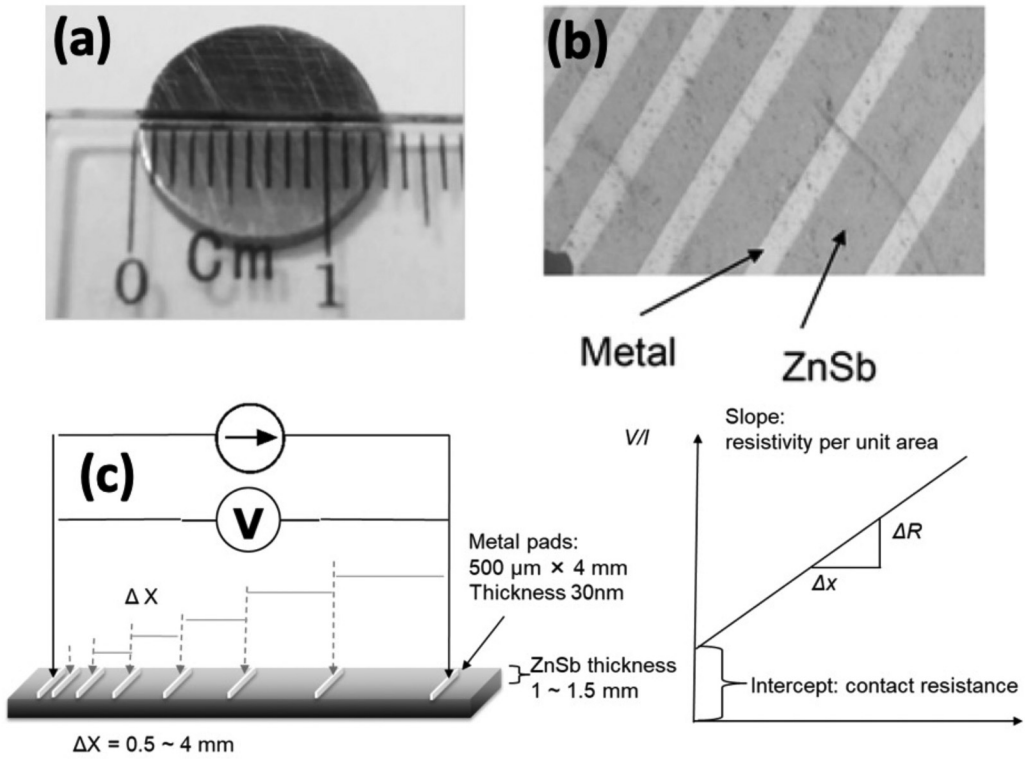

FIG. 3. Demonstration of contact resistance measurement: (a) ZnSb substrate by hot-pressing and (b) scanning electron microscope image of metal stripes created by a shadow mask during deposition. (c) IV measurement across two neighboring metal pads is shown on the left sketch. The measured resistance is then plotted vs contact interval is shown in the plot on the right hand where the contact resistance is determined.

seen in Fig. 4(b). We comment that we do not know if the adhesion problems seen in Fig. 4(a) are enhanced for the ZnSb/Cu system, by the deposition method, or the vacuum condition of the equipment.

The Ti/ZnSb interface for e-gun evaporated Ti deposited films also appears smooth (Fig. 5). The details of the structure of the interface will be presented in detail elsewhere,[20] while we here focus on the electrical properties of the ZnSb–metal interface.

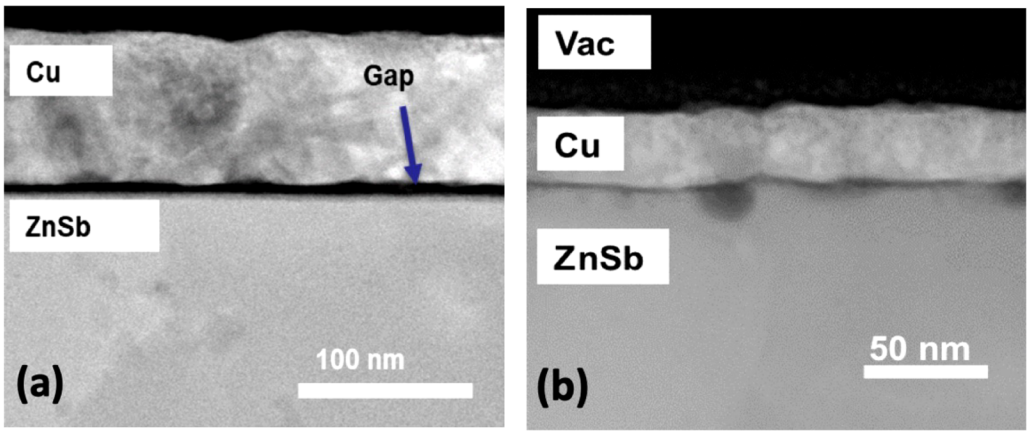

FIG. 4. Transmission electron microscope image of Cu/ZnSb where Cu is deposited by (a) e-beam evaporator and (b) magnetron sputtering.

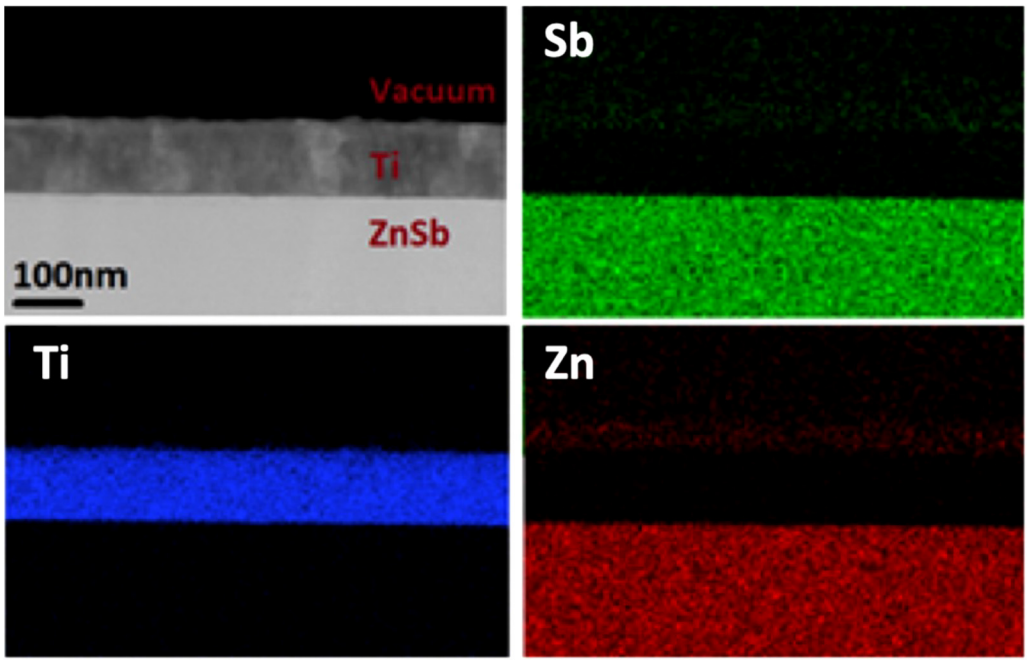

FIG. 5. Annular dark-field transmission electron microscopic (ADF-TEM) image and energy dispersive x-ray spectrometry (EDS) micrograph of the interface between Ti and ZnSb.

B. Contact resistance and electronic properties

1. Cu/ZnSb interface

Figure 6 shows an example of contact resistance measurements for a ZnSb substrate doped with 0.1 at. % Cu, with a sputter deposited Cu contact film heat treated for 3 h at different temperatures as annotated. We see from the figure that the resistance values in the plot fall on straight lines for the different samples. The contact resistance is deduced from the intercept with the ordinate axis, while the slope of the curves is related to the resistivity of the substrate. We observe that the slopes become less steep with increasing annealing temperature, indicating that the resistivity of the substrate was decreased by annealing. This is consistent with the measured carrier concentration, which also was altered by annealing. This is probably associated with the generation of Zn vacancy related point defects by annealing. Zn vacancies act as acceptors in ZnSb[3,21–23] and also interact with dopants and impurities.

We include the deduced specific contact resistance in an overview over the measurements containing all the sputtered Cu films. This is shown in Fig. 7 where the specific contact resistance is plotted as a function of the carrier concentration. The top abscissa of the figure shows the measured Hall carrier concentration, while the bottom abscissa shows $N_A^{-\frac{1}{2}}$, assuming that the carrier concentration is equal to the acceptor concentration. Several samples were damaged after heat treatment at 300 °C, we therefore only show results up to 258 °C.

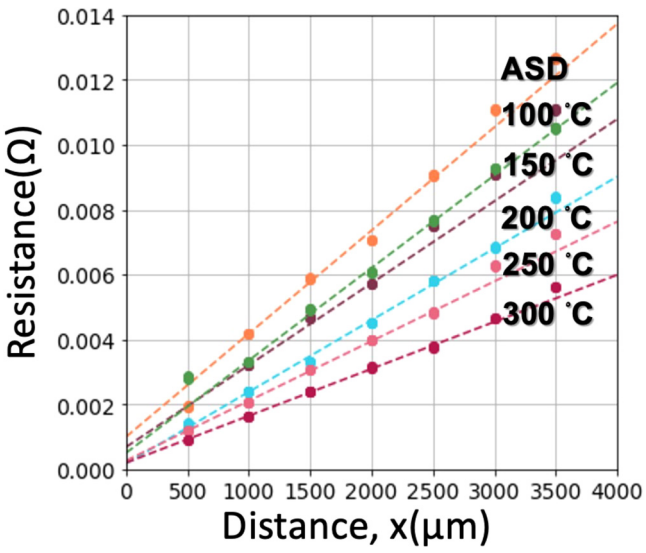

FIG. 6. Example of measured resistance vs distance between contacts, x. Here for a Cu film on ZnSb doped with 0.1 at. % Cu. The data for the as-deposited case are labeled ASD and the data for the annealed cases are labeled with the respective annealing temperature for 3 h. The data are used to determine the contact resistance.

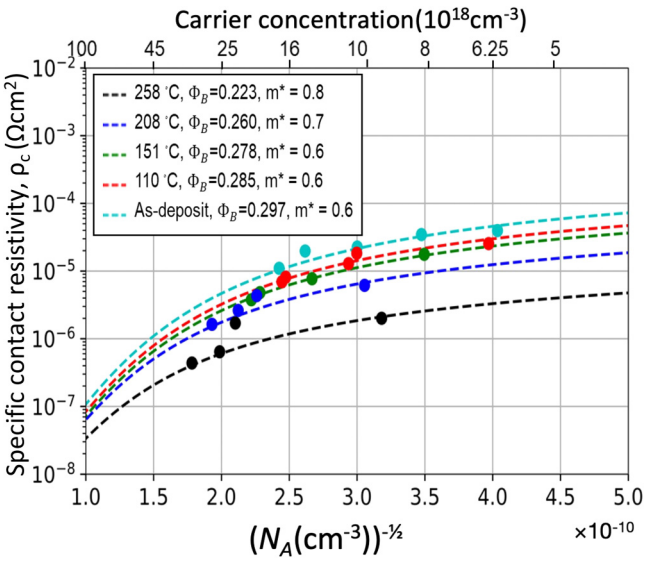

FIG. 7. Specific contact resistance vs the charge carrier concentration of substrate, after heat treated at different temperatures. The different colors indicate the annealed temperature, while at each temperature the scatters indicate the different samples with various charge carrier concentrations. The dashed lines are the plot of Eq. (1).

It is seen from Fig. 7 that the specific contact resistance of all the Cu/ZnSb contacts is in the range of 10^{-7}–10^{-5} Ω cm^2. In regard to the estimation of power loss shown in Fig. 1(d), the range of specific contact resistance of Fig. 7 implies that the power loss at such contacts can be below 10%. The data points for different annealing temperatures have been given different colors. The dashed lines in Fig. 7 are fits to the theory given by Yu[17] incorporating the combination of three different emission mechanisms (TE, TFE, and FE) across the metal–semiconductor barrier. The explicit dependence on the doping concentration for the FE, TFE, and TE was given in Eq. (1). The measured data fit the model where thermionic-field emission dominates. It is seen that the measured data points tend to merge as the doping concentration gets higher. That is in agreement with the theory and indicates that the contact resistance is dominated by the doping concentration and that differences in barrier height play a diminishing role. The scatters in the same color in Fig. 7 represent each sample with different Cu concentrations.

The barrier height Φ_{Bp} and the density of states effective mass m^* are fitting parameters for each of the dotted lines in Fig. 7. Here, Φ_{Bp} has a range of 0.22–0.3 eV. Although there are no reports on the barrier height for ZnSb, these values seem plausible considering that the bandgap of ZnSb is about 0.5 eV.[3,24] Furthermore, there is a tendency for covalent semiconductors to have a barrier height such that the Fermi level is "pinned" within the bandgap. However, this is not demanded by any physical or chemical laws and exceptions exist.[16] Here, we conclude that the present measurement data of Fig. 7 should not be regarded as a measurement of barrier heights, but the data trends of the data may have a functional dependence that is predicted by the applied model. As for the effective mass that is used for the fits in Fig. 7, they have values between 0.6 and 0.8. These are also reasonable values, as we note that it has been reported values in this range from other experiments on ZnSb.[15,25]

While the range of measured values of Fig. 7 seems reasonable, and the overall shape of the data set is qualitatively in agreement with the applied transport model, there also seem to be systematic trends in the fitted curves with respect to the annealing temperatures. We will here consider these systematics and suggest a physical interpretation of the apparent trends, while keeping in mind that the theory was formulated in order to have tractable expressions and not to have the most accurate calculations from first principles nor a high numerical accuracy.

First, we see the curves representing the different lines for different annealing temperatures are associated with a fitted barrier height that decreases with increasing annealing temperature. This trend is plotted in Fig. 8. A change in barrier height is, in general, accompanied by a change in electrical dipole at the interface, which could be realized by a transfer of electric charge by electrons. It is likely that there are changes in the interface as a result of annealing; atoms rearrange, and new bonding between interface atoms occurs. Thus, new localized quantum states are created or removed and a change in the electric dipole can occur with a concomitant change in the barrier height. It may also mean that when the electron quantum states of the interface states change, the energy position of the Fermi level giving electrical neutrality to the system will change. That can be referred to as a change in the Fermi level pinning at the interface. This scenario is schematically illustrated in Fig. 9.

We will now discuss the apparent trend that the effective mass is dependent on the annealing temperature, also plotted in Fig. 8. It is correlated with a variation of the barrier height and can be directly linked to it. A qualitative explanation for that is proposed by reference to Fig. 9 showing spatial energy diagrams for a low annealing temperature case to the left and that for a high annealing temperature case in the middle. We consider that the dominant transport is in the TFE region where the dominating transport mechanism is tunneling through the tip of the barrier by carriers

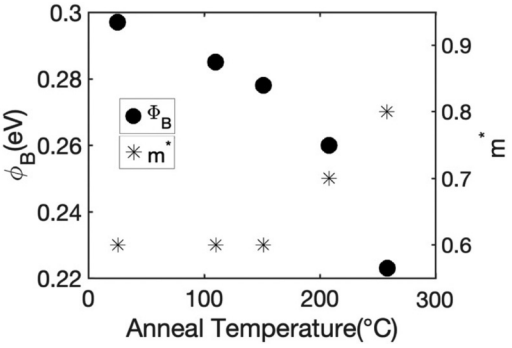

FIG. 8. The fitting parameters Φ_B and m^* derived from contact measurement in Fig. 7 vs the anneal temperature. Φ_B is the barrier height and m^* is the effective mass.

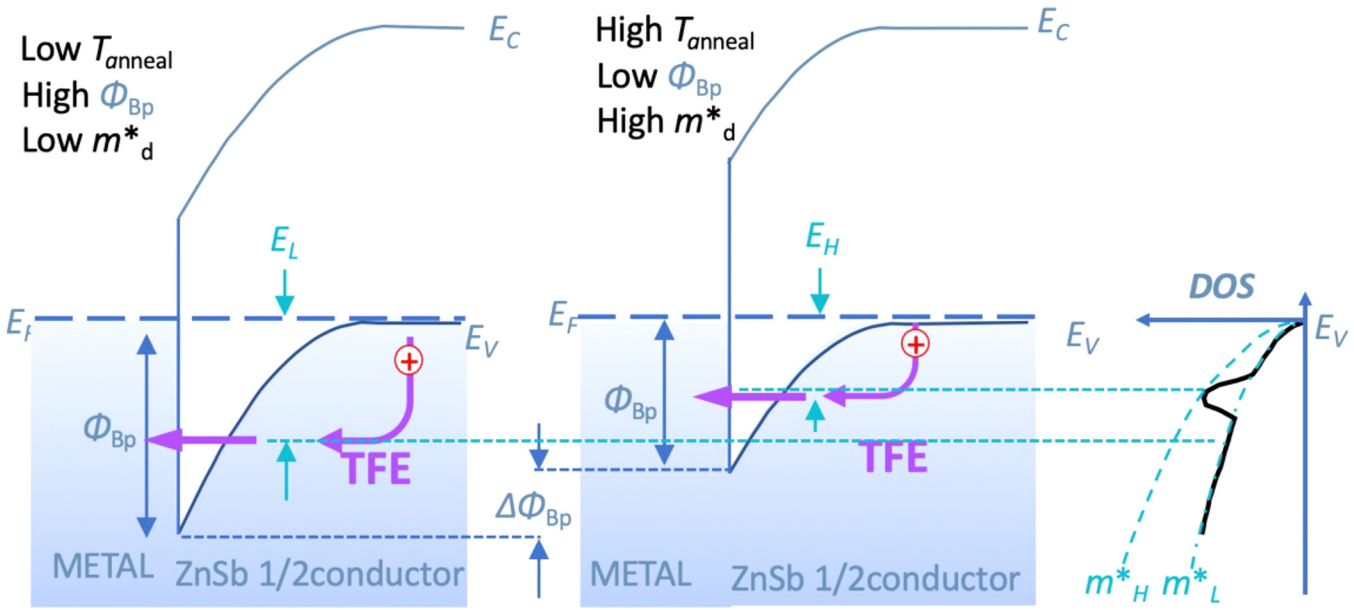

FIG. 9. Schematic drawing of a metal to p-type semiconductor junction, illustrating reasons for the trend seen in Fig. 8. The effects are exaugurated in the schematics. Both figures show alignment of the energy bands for zero bias. Going from the left to the right, there is a change in the electric dipole at the metal–semiconductor transition. This change will cause a change in the barrier height. The change was induced by annealing, which could cause a change in the interface state density and energy distribution. It would change the interface neutral layer and, therefore, the barrier height resulting in $\Delta\Phi_{Bp}$.

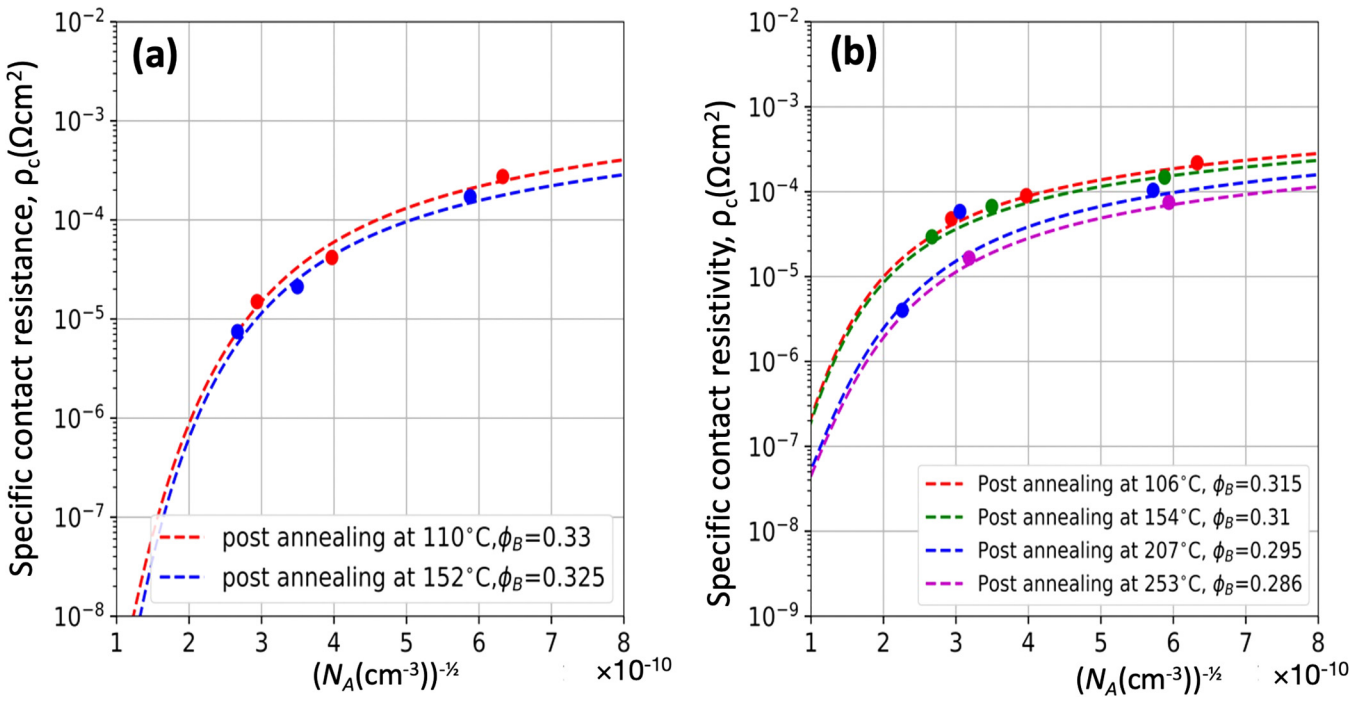

FIG. 10. The specific contact resistance of (a) Ti and (b) Ni on ZnSb fitted with Eq. (1).

(holes) that are thermally excited to where the barrier is thin enough to give appreciable tunneling. There will thus be an energy range where the majority of the transported carriers will tunnel. That is illustrated in Fig. 9 by a heavily drawn arrow going to the left through the barrier. The energy position of this will be different for the two annealing temperatures, indicated by the energy difference E_H and E_L for the high and low annealing temperature cases, respectively. The kinetic energy for the carriers at the arrow for the low temperature annealing case is higher than that for the high temperature case. This means that there are different states involved in the two cases. These states may have a different effective mass for a semiconductor that do not follow/comply to the single band (SPB) idealization. In the case of ZnSb, it has been reported that it deviates from a SPB description.[15,25] An example of features in the density of states, DOS, that would represent a different effective mass for the two cases is shown schematically rightmost in Fig. 9. There is the energy region where tunneling dominates for the low temperature case falls in a region of the DOS where the effective mass would be assigned a low value m^*_L, whereas for the high temperature case it would fall in a region assigned a high effective mass.

2. Contact resistance of Ti and Ni on ZnSb

The specific contact resistances of Ti and Ni on ZnSb are also fitted with Eq. (1), shown in Fig. 10. The specific contact resistance of both metals is in the range of 10^{-5}–$10^{-4}\,\Omega\,\mathrm{cm}^2$, where the power loss at contact is about 20%–40%. These values are higher than for the case of sputtered Cu. The variation of the fitting parameters is smaller. This may reflect that the changes in the interface for the parameter space applied are smaller than for the case of Cu. However, the number of measurements is more limited. Further expansion of anneal temperature ranges could reveal interesting features and be important for thermoelectric applications.

V. CONCLUDING REMARKS

In the present work, we have deposited metal films on hot-pressed ZnSb substrates and studied the contact resistance of the metal–ZnSb interface after heat treatments. In order to compare the electronic properties, the substrates were doped with Cu to different concentrations to study the details of the transport mechanisms at the interface. The specific contract resistance decreases after annealing at increasing temperatures and was in the range of 10^{-7}–$10^{-5}\,\Omega\,\mathrm{cm}^2$, which indicates a power loss at contact of 10% or less. The values of the measured contact resistance were fitted and analyzed with an existing metal–semiconductor contact resistance model. We discussed the validity of the model and its ability to reveal trends related to the chemistry changes in the Cu/ZnSb interface influencing charge carrier transport and proposed a description that could be an inspiration to further studies on the system at hand and others. The hypothetic description which is in agreement with the experiment is that for Cu/ZnSb the barrier height decreases with increasing annealing temperature and the resulting variation in contact resistance indicates a non-parabolic valence band.

ACKNOWLEDGMENTS

The Research Council of Norway is acknowledged for the support of the Norwegian Micro- and Nano-Fabrication Facility, NorFab, Project No. 295864; the Norwegian Center for Transmission Electron Microscopy, NORTEM, Project No. 197405; and NEAT, Project No. 262339.

DATA AVAILABILITY

The data that support the findings of this study are available from the corresponding author upon reasonable request.

REFERENCES

[1]D. Beretta, N. Neophytou, J. M. Hodges, M. G. Kanatzidis, D. Narducci, M. Martin- Gonzalez, M. Beekman, B. Balke, G. Cerretti, W. Tremel, A. Zevalkink, A. I. Hofmann, C. Müller, B. Dörling, M. Campoy-Quiles, and M. Caironi, Mater. Sci. Eng., R **138**, 100501 (2019).
[2]M. G. Farmer, U.S. patent 109,603A (29 November 1870).
[3]X. Song and T. G. Finstad, "Ch. 6, Review of research on the thermoelectric material ZnSb," in *Thermoelectrics for Power Generation: A Look at Trends in the Technology* (InTech, Rijeka, 2016).
[4]J. H. Goldsmid, *Introduction to Thermoelectricity* (Springer, 2009), p. 23.
[5]K. Valset, P. H. M. Bottger, J. Tafto, and T. G. Finstad, J. Appl. Phys. **111**, 023703 (2012).
[6]M. I. Fedorov, L. V. Prokof'eva, D. A. Pshenay-Severin, A. A. Shabaldin, and P. P. Konstantinov, J. Electron. Mater. **43**, 2314 (2014).
[7]D.-B. Xiong, N. L. Okamoto, and H. Inui, Scr. Mater. **69**, 397 (2013).
[8]R. Pothin, R. M. Ayral, A. Berche, D. Granier, F. Rouessac, and P. Jund, Chem. Eng. J. **299**, 126 (2016).
[9]L. Song, J. Zhang, and B. B. Iversen, ACS Appl. Energy Mater. **3**, 2055 (2020).
[10]J. Yoon, S. H. Bae, H.-S. Sohn, I. Son, K. T. Kim, and Y.-W. Ju, J. Nanosci. Nanotechnol. **18**, 6515 (2018).
[11]Y. I. Shtern, R. E. Mironov, M. Y. Shtern, A. A. Sherchenkov, and M. S. Rogachev, Acta Phys. Pol. A **129**, 785 (2016).
[12]D. H. Jung, A. Sharma, M. Mayer, and J. P. Jung, Rev. Adv. Mater. Sci. **53**, 147 (2018).
[13]S. Abbas Malik, L. Thanh Hung, and N. Van Nong, Mater. Today: Proc. **8**, 625 (2019).
[14]M. Yin, A. Zhong, J. Luo, F. Li, Z. Zheng, and P. Fan, J. Electron. Mater. **46**, 3256 (2017).
[15]K. Valset, X. Song, and T. G. Finstad, J. Appl. Phys. **117**, 045709 (2015).
[16]R. Tung, Appl. Phys. Rev. **1**, 011304 (2014).
[17]A. Y. C. Yu, Solid State Electron. **13**, 239 (1970).
[18]See https://www.norfab.no/lab-facilities/uio-minalab/ for NorFab_UiO_MinaLab (2021).
[19]D. K. Schroder, *Semiconductor Material and Device Characterization* (John Wiley & Sons, 2006).
[20]H. Riis, X. Song, T. G. Finstad, and Ø. Prytz, "Metallization of ZnSb with Cu, Ti and Al: A study of chemical composition and contact resistance" (unpublished) (2021).
[21]X. Song, M. Schrade, N. Masó, and T. G. Finstad, J. Alloys Compd. **710**, 762 (2017).
[22]L. Bjerg, G. K. H. Madsen, and B. B. Iversen, Chem. Mater. **24**, 2111 (2012).
[23]P. Jund, R. Viennois, X. Tao, K. Niedziolka, and J.-C. Tédenac, Phys. Rev. B **85**, 225105 (2012).
[24]P. J. Shaver and J. Blair, Phys. Rev. **141**, 649 (1966).
[25]P. H. M. Bottger, G. S. Pomrehn, G. J. Snyder, and T. G. Finstad, Phys. Status Solidi A **208**, 2753 (2011).